

ChemCatChem

Alkene Hydrosilylation on Oxide-supported Pt-ligand Single-site Catalysts

--Manuscript Draft--

Manuscript Number:	
Article Type:	Full Paper
Corresponding Author:	Steven L Tait Indiana University Bloomington, UNITED STATES
Corresponding Author E-Mail:	tait@indiana.edu
Order of Authors (with Contributor Roles):	Linxiao Chen lyad S. Ali George E. Sterbinsky Jocelyn T. L. Gamler Sara E. Skrabalak Steven L Tait
Keywords:	single-site heterogeneous catalyst; hydrosilylation; platinum; X-ray photoelectron spectroscopy; X-ray absorption spectroscopy
Manuscript Classifications:	Heterogeneous catalysis; Hydrosilylation; N ligands; Supported catalysts
Suggested Reviewers:	<p>Rick Finke Colorado State University Walter Scott Jr College of Engineering Richard.Finke@colostate.edu Expertise in heterogeneous catalysis and hydrosilylation reactions.</p> <p>Yadong Li Tsinghua University ydli@mail.tsinghua.edu.cn His group has published two recent papers (2018) on using Pt SSCs for hydrosilylation reactions.</p> <p>Fritz Kuhn Technische Universitat Munchen fritz.kuehn@ch.tum.de Published recent paper (2016) on hydrosilylation mechanism, relevant to this work.</p> <p>Chloé Thieuleux Universite de Lyon thieuleux@cpe.fr Recent work (2012) on heterogeneous Pt catalysts (nanoparticles) for hydrosilylation.</p>
Opposed Reviewers:	
Abstract:	<p>Heterogeneous single-site catalysts (SSCs), widely regarded as promising next-generation catalysts, blend the easy recovery of traditional heterogeneous catalysts with desired features of homogeneous catalysts: high fraction of active sites and uniform metal centers. We previously reported the synthesis of Pt-ligand SSCs through a novel metal-ligand self-assembly method on MgO, CeO₂, and Al₂O₃ supports (J. Catal. 2018, 365, 303-312). Here, we present their applications in the industrially-relevant alkene hydrosilylation reaction, with 95% yield under mild conditions. The comparison with commercial catalysts (Karstedt and Speier) reveals several advantages of these SSCs: higher selectivity, less colloidal Pt formation, less alkene isomerization/hydrogenation, and better tolerance towards functional groups in substrates. Despite some leaching, our catalysts exhibit satisfactory recyclability and the single-site structure remains intact on oxide supports after reaction. Pt single-sites are shown to be the main active sites rather than colloidal Pt formed during the reaction. An induction period is observed in which Pt sites are activated by Cl detachment and replacement by reactant alkenes. Catalytic performance of Pt SSCs is</p>

	sensitive to the ligand and support choices. This work highlights the application of heterogeneous metal-ligand SSCs in an industrially-relevant reaction with several improvements over current commercial catalysts.
Author Comments:	This manuscript presents a detailed investigation of alkene hydrosilylation catalysis using a Pt-ligand single-site catalysts (SSCs) on oxide powder supports. This class of metal-ligand SSC has been recently developed by our group and here we report the first detailed study showing its catalytic activity and stability during hydrosilylation reactions. SSCs are of significant interests due to high active site fraction and reaction selectivity, yet their availability and application are challenged by the inherently instable nature of single metal atoms. Our metal-ligand assembly strategy uses ligands with attractive metal binding pockets and good oxidizing potential to stabilize SSCs. The catalysts reported in this manuscript show significant advantages over commercial hydrosilylation (metal nanoparticle) catalysts in several crucial aspects, as well as sensitivity to ligand and support design, opening new opportunities for upgrading important industrial processes. This manuscript also examines how metal single-sites evolve under catalytic conditions, helping to elucidate SSC mechanisms and enhance stability. These results will be of interest to the readership of the ChemCatChem due to the novelty of the catalyst design, their advantages in an industrially significant reaction, and the fundamental insights into the behavior of metal single-sites during catalytic processes.
Section/Category:	
Additional Information:	
Question	Response
Submitted solely to this journal?	Yes
Has there been a previous version?	No
Do you or any of your co-authors have a conflict of interest to declare?	No. The authors declare no conflict of interest.
Animal/tissue experiments?	No

1
2
3
4
5
6
7
8
9
10
11
12
13
14
15
16
17
18
19
20
21
22
23
24
25
26
27
28
29
30
31
32
33
34
35
36
37
38
39
40
41
42
43
44
45
46
47
48
49
50
51
52
53
54
55
56
57
58
59
60
61
62
63
64
65

For submission to ChemCatChem

Alkene Hydrosilylation on Oxide-supported Pt-ligand Single-site Catalysts

Linxiao Chen,^[a] Iyad S. Ali,^[a] George E. Sterbinsky,^[b] Jocelyn T. L. Gamler,^[a] Sara E.
Skrabalak,^[a] and Steven L. Tait*^[a]

[a] L. Chen, I. S. Ali, J. T. L. Gamler, Prof. S. E. Skrabalak, Prof. S. L. Tait

Department of Chemistry

Indiana University

800 E. Kirkwood Ave., Bloomington, Indiana 47405 (U. S. A.)

E-mail: tait@indiana.edu

[b] Dr. G. E. Sterbinsky

Advanced Photon Source,

Argonne National Laboratory

9700 S. Cass Ave., Lemont, Illinois 60439 (U. S. A.)

1
2
3
4 **Abstract**
5
6

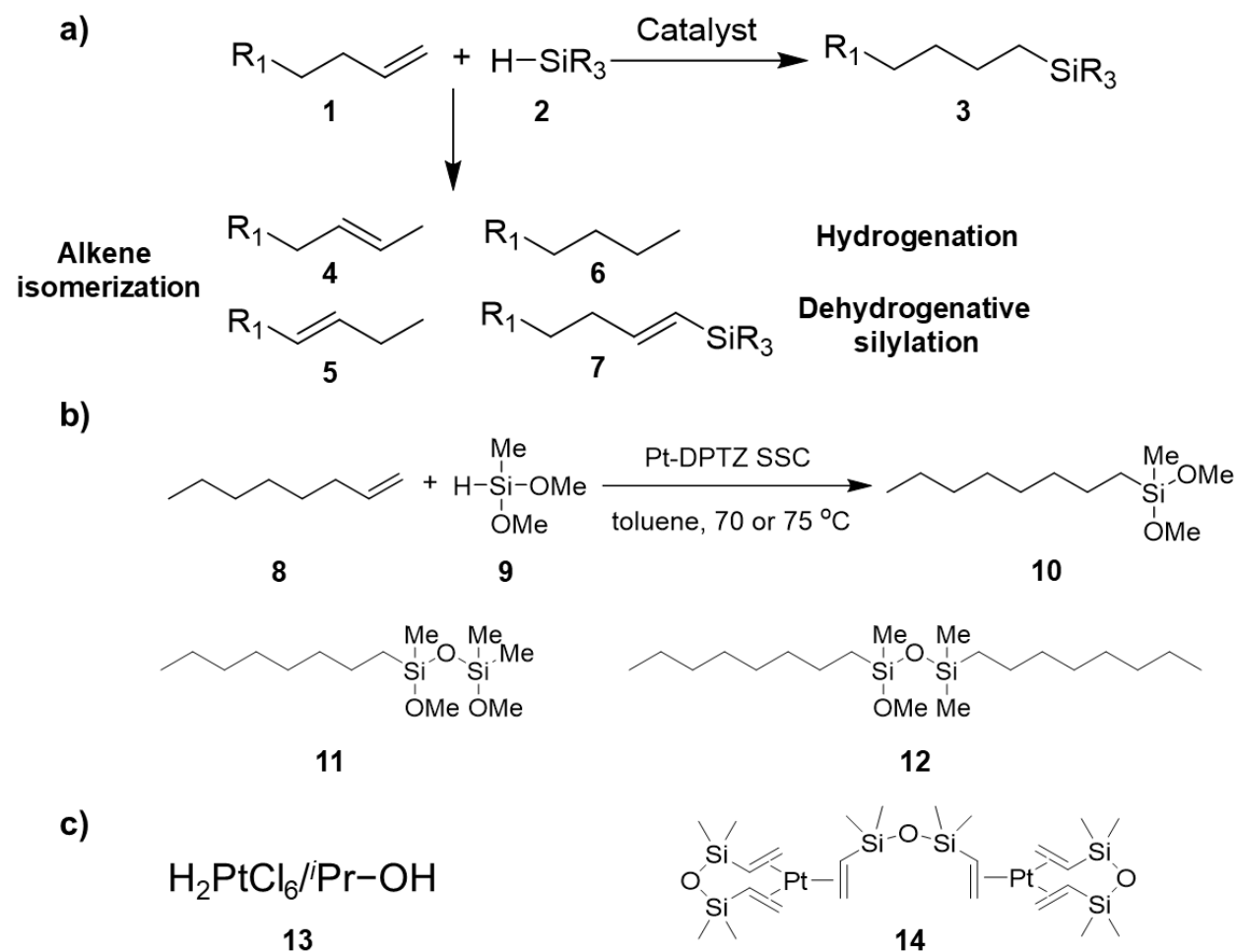
7 Heterogeneous single-site catalysts (SSCs), widely regarded as promising next-generation
8 catalysts, blend the easy recovery of traditional heterogeneous catalysts with desired features of
9 homogeneous catalysts: high fraction of active sites and uniform metal centers. We previously
10 reported the synthesis of Pt-ligand SSCs through a novel metal-ligand self-assembly method on
11 MgO, CeO₂, and Al₂O₃ supports (*J. Catal.* **2018**, *365*, 303-312). Here, we present their
12 applications in the industrially-relevant alkene hydrosilylation reaction, with 95% yield under
13 mild conditions. The comparison with commercial catalysts (Karstedt and Speier) reveals several
14 advantages of these SSCs: higher selectivity, less colloidal Pt formation, less alkene
15 isomerization/hydrogenation, and better tolerance towards functional groups in substrates.
16 Despite some leaching, our catalysts exhibit satisfactory recyclability and the single-site structure
17 remains intact on oxide supports after reaction. Pt single-sites are shown to be the main active
18 sites rather than colloidal Pt formed during the reaction. An induction period is observed in
19 which Pt sites are activated by Cl detachment and replacement by reactant alkenes. Catalytic
20 performance of Pt SSCs is sensitive to the ligand and support choices. This work highlights the
21 application of heterogeneous metal-ligand SSCs in an industrially-relevant reaction with several
22 improvements over current commercial catalysts.
23
24
25
26
27
28
29
30
31
32
33
34
35
36
37
38
39
40
41
42
43
44
45
46
47
48
49
50
51
52
53
54
55
56
57
58
59
60
61
62
63
64
65

Introduction

Catalytic hydrosilylation, the addition of silicon hydrides (**2**, Scheme 1) (Si–H bonds) to multiple bonds (particularly C=C or C≡C bonds, **1**), has been one of the most important reactions in silicon chemistry. Since its first report in 1947,^[1] hydrosilylation has been extended to a broad range of unsaturated substrates. It has been widely applied in industry to functionalize silicone polymers and other silica-based materials, to produce diverse materials with desired physiochemical properties.^[2] These functionalized materials are of paramount importance in manufacturing diverse commodities, such as resins, lubricant oils, and coatings.^[3] Catalytic hydrosilylation itself is also an efficient method to create silica-containing polymers as preceramic,^[4] adhesive,^[5] and sealing materials.^[6] Furthermore, the cross-linking between multi-hydride and multi-vinyl silicone polymers provides a technology for silicone curing (elastomers, coatings).^[3a, 7] Aside from heavy application in polymer industry, catalytic hydrosilylation of silane monomers also attracts significant interests, as it is a versatile synthetic tool to generate Si–C building blocks in fine chemical synthesis.^[8]

Most industrial hydrosilylation processes use homogeneous Pt complex catalysts. In the late 1950s, Speier discovered that the H₂PtCl₆/Pr–OH system (**13**) is an effective hydrosilylation catalyst with vastly improved selectivity.^[9] It was the most commonly used industrial catalyst, until being replaced by the more active and selective Karstedt catalyst and its derivatives. The Karstedt catalyst (**14**), a platinum(0) complex containing vinyl-siloxane ligands that was initially reported in 1973,^[10] is still the benchmark for hydrosilylation activity. Other metals, such as Rh, Ir, Fe, Ru, Ni, Ti, and Re,^[11] as well as non-metal catalyst (boron/phosphorus-based)^[12] have also been explored due to concerns with the use of Pt, including side reactions (selectivity), high cost, volatile market, and uncertainty in the future supply of Pt. However, none of these alternatives

1
2
3
4 have been able to match the hydrosilylation activity of Pt, so it seems likely that the industry will
5
6 largely rely on Pt catalysts for a considerable amount of time. Current investigations remain
7
8 focused on improving Pt-based catalysts, aiming to develop more efficient and stable catalysts
9
10 with lower cost.^[13]
11
12
13



Scheme 1. Alkene hydrosilylation reactions and catalysts. **(a)** General representation of alkene hydrosilylation reactions and potential side reactions. A wide variety of side chains can be selected for the silane positions (R, not necessarily all the same) and alkene (R_1) to design the desired properties of the final product. **(b)** The hydrosilylation reaction performed in this work between 1-octene (**8**) and dimethoxymethyl silane (**9**), as well as the main Si-containing byproducts detected by GC-MS (**11**, **12**). **(c)** Structures of the Speier (**13**) and Karstedt (**14**) catalysts (commercial homogeneous catalysts).

1
2
3
4 Drawbacks of current commercial catalysts include the aggregation of Pt centers into colloids
5
6 and multiple side reactions from C=C bonds. Despite some reports stating that colloidal Pt also
7
8 catalyze hydrosilylation,^[14] the dominant opinion is that Pt aggregation leads to deactivation.^{[3a,}
9
10
11^{15]} Most Pt catalysts also catalyze alkene isomerization, hydrogenation, and dehydrogenative
12
13 silylation reactions that yield byproducts **4-7**. Recently, motivated by the early work of Marko, *et*
14
15 *al.*, with N-heterocyclic carbene,^[13a, 13b] platinum-carbene complexes have been explored
16
17 extensively as potential replacements that provide better stability.^[16] Other endeavors include
18
19 trinuclear Pt(0) catalysts with alkyne ligands,^[17] and anti-sulfur-poisoning Pt catalysts.^[18]
20
21 Heterogeneous Pt catalysts have been applied to this reaction as well, including Pt(0)
22
23 nanoparticles,^[14] PtO₂,^[13c] and supported Pt single-sites.^[19] The initial mechanism model for
24
25 alkene hydrosilylation was proposed by Chalk and Harrod in 1965, and has enjoyed great
26
27 acceptance since then (Figure S1).^[20] The oxidative addition of silane occurs first on Pt centers,
28
29 and then C=C bond coordinates with Pt. The migratory insertion of C=C bonds to Si-H bonds
30
31 and the subsequent reductive elimination from Pt eventually yield products. A modified Chalk-
32
33 Harrod mechanism was later proposed including the insertion of unsaturated substrates to Pt-Si
34
35 bond,^[21] but has been shown recently to be unfavorable to the original Chalk-Harrod
36
37 mechanism.^[22]

38
39
40
41
42
43
44
45
46 Heterogeneous single-site catalysts (SSCs) have attracted attentions across the catalysis
47
48 community as a strategy to combine advantages of homogeneous and heterogeneous catalysts.^[23]
49
50
51
52
53
54
55
56
57
58
59
60
61
62
63
64
65
66
67
68
69
70
71
72
73
74
75
76
77
78
79
80
81
82
83
84
85
86
87
88
89
90
91
92
93
94
95
96
97
98
99
100
101
102
103
104
105
106
107
108
109
110
111
112
113
114
115
116
117
118
119
120
121
122
123
124
125
126
127
128
129
130
131
132
133
134
135
136
137
138
139
140
141
142
143
144
145
146
147
148
149
150
151
152
153
154
155
156
157
158
159
160
161
162
163
164
165
166
167
168
169
170
171
172
173
174
175
176
177
178
179
180
181
182
183
184
185
186
187
188
189
190
191
192
193
194
195
196
197
198
199
200
201
202
203
204
205
206
207
208
209
210
211
212
213
214
215
216
217
218
219
220
221
222
223
224
225
226
227
228
229
230
231
232
233
234
235
236
237
238
239
240
241
242
243
244
245
246
247
248
249
250
251
252
253
254
255
256
257
258
259
260
261
262
263
264
265
266
267
268
269
270
271
272
273
274
275
276
277
278
279
280
281
282
283
284
285
286
287
288
289
290
291
292
293
294
295
296
297
298
299
300
301
302
303
304
305
306
307
308
309
310
311
312
313
314
315
316
317
318
319
320
321
322
323
324
325
326
327
328
329
330
331
332
333
334
335
336
337
338
339
340
341
342
343
344
345
346
347
348
349
350
351
352
353
354
355
356
357
358
359
360
361
362
363
364
365
366
367
368
369
370
371
372
373
374
375
376
377
378
379
380
381
382
383
384
385
386
387
388
389
390
391
392
393
394
395
396
397
398
399
400
401
402
403
404
405
406
407
408
409
410
411
412
413
414
415
416
417
418
419
420
421
422
423
424
425
426
427
428
429
430
431
432
433
434
435
436
437
438
439
440
441
442
443
444
445
446
447
448
449
450
451
452
453
454
455
456
457
458
459
460
461
462
463
464
465
466
467
468
469
470
471
472
473
474
475
476
477
478
479
480
481
482
483
484
485
486
487
488
489
490
491
492
493
494
495
496
497
498
499
500
501
502
503
504
505
506
507
508
509
510
511
512
513
514
515
516
517
518
519
520
521
522
523
524
525
526
527
528
529
530
531
532
533
534
535
536
537
538
539
540
541
542
543
544
545
546
547
548
549
550
551
552
553
554
555
556
557
558
559
560
561
562
563
564
565
566
567
568
569
570
571
572
573
574
575
576
577
578
579
580
581
582
583
584
585
586
587
588
589
590
591
592
593
594
595
596
597
598
599
600
601
602
603
604
605
606
607
608
609
610
611
612
613
614
615
616
617
618
619
620
621
622
623
624
625
626
627
628
629
630
631
632
633
634
635
636
637
638
639
640
641
642
643
644
645
646
647
648
649
650
651
652
653
654
655
656
657
658
659
660
661
662
663
664
665
666
667
668
669
670
671
672
673
674
675
676
677
678
679
680
681
682
683
684
685
686
687
688
689
690
691
692
693
694
695
696
697
698
699
700
701
702
703
704
705
706
707
708
709
710
711
712
713
714
715
716
717
718
719
720
721
722
723
724
725
726
727
728
729
730
731
732
733
734
735
736
737
738
739
740
741
742
743
744
745
746
747
748
749
750
751
752
753
754
755
756
757
758
759
760
761
762
763
764
765
766
767
768
769
770
771
772
773
774
775
776
777
778
779
780
781
782
783
784
785
786
787
788
789
790
791
792
793
794
795
796
797
798
799
800
801
802
803
804
805
806
807
808
809
810
811
812
813
814
815
816
817
818
819
820
821
822
823
824
825
826
827
828
829
830
831
832
833
834
835
836
837
838
839
840
841
842
843
844
845
846
847
848
849
850
851
852
853
854
855
856
857
858
859
860
861
862
863
864
865
866
867
868
869
870
871
872
873
874
875
876
877
878
879
880
881
882
883
884
885
886
887
888
889
890
891
892
893
894
895
896
897
898
899
900
901
902
903
904
905
906
907
908
909
910
911
912
913
914
915
916
917
918
919
920
921
922
923
924
925
926
927
928
929
930
931
932
933
934
935
936
937
938
939
940
941
942
943
944
945
946
947
948
949
950
951
952
953
954
955
956
957
958
959
960
961
962
963
964
965
966
967
968
969
970
971
972
973
974
975
976
977
978
979
980
981
982
983
984
985
986
987
988
989
990
991
992
993
994
995
996
997
998
999
1000

1
2
3
4 separation. SSCs have proved effective in gas phase and solution phase reactions, including
5
6 hydrosilylation (Pt^{δ+}/TiO₂ and Pt/graphene SSCs).^[19, 24]
7
8

9
10 Previous work from our group established a novel SSC synthesis strategy using metal-ligand
11 self-assembly on powdered oxide supports.^[25] The development of these systems was based on
12 well-controlled model systems on single crystal surfaces in ultra-high vacuum.^[26] On multiple
13
14 powdered oxide supports, Pt can be atomically dispersed in oxidized Pt(II) form between N
15 binding pockets, stabilized by the oxidizing ability of the 3,6-Di-2-pyridyl-1,2,4,5-tetrazine
16
17 (DPTZ) ligand (Figures 1a, 1b).^[25]
18
19
20
21
22
23
24

25 In this work, we report detailed investigations into alkene hydrosilylation using these oxide-
26 supported Pt-DPTZ SSCs. Satisfactory yield was achieved under mild conditions for several
27 catalytic cycles, with higher activity per Pt site than traditional nanoparticle catalysts. Compared
28
29 with commercial catalysts, supported Pt-DPTZ SSCs are not only easier to recycle, but also
30 provide higher yield, less colloidal Pt, fewer byproducts from alkene, and improved tolerance to
31 epoxy groups in substrates. The evolution of Pt single-sites, including leaching from the support
32 to aggregate into colloidal Pt in solution during the reaction as well as active site formation
33 during the induction period or pretreatment, was systematically explored to better understand Pt
34 behavior during catalysis. This is the first report using SSCs synthesized from the metal-ligand
35 self-assembly strategy for industrially relevant reactions. Their effectiveness in alkene
36
37 hydrosilylation catalysis and improvements over current commercial catalysts offer practical
38
39 advantages.
40
41
42
43
44
45
46
47
48
49
50
51
52
53
54
55
56
57
58
59
60
61
62
63
64
65

Results and Discussions

1
2
3
4
5
6
7
8
9
10
11
12
13
14
15
16
17
18
19
20
21
22
23
24
25
26
27
28
29
30
31
32
33
34
35
36
37
38
39
40
41
42
43
44
45
46
47
48
49
50
51
52
53
54
55
56
57
58
59
60
61
62
63
64
65

1. **Catalytic performance of Pt-DPTZ single-site catalysts (SSCs).** The synthesis of oxide-supported Pt-DPTZ SSCs was previously reported by our group.^[25] Pt(II) single-sites were created using metal-ligand self-assembly, taking advantage of the favorable N binding pockets in DPTZ (Figure 1a) and its electron-accepting potential that stabilizes isolated Pt cations. The simultaneous impregnation of Pt precursor $\text{H}_2\text{PtCl}_6 \cdot 6\text{H}_2\text{O}$ and DPTZ onto MgO, CeO_2 , or Al_2O_3 powders generated Pt-DPTZ single-site structures (Figure 1b), in which Pt also interacts with O from oxide supports (not shown in drawing). The single-site nature of Pt was confirmed by the extended X-ray absorption fine structure (EXAFS) region of X-ray absorption spectroscopy (XAS, Figure 1c) and other techniques (Figure S2). X-ray photoemission spectroscopy (XPS) shows that > 90% Pt sites exist as Pt(II) complexes, and the formation of metallic Pt nanoparticles (NP, zero valent) or mixed Pt(IV) oxide (on MgO) are almost completely prevented (Figure 1d). Besides the structure shown in Figure 1b, the formation of PtO_xCl_y single-sites cannot be eliminated, especially on CeO_2 , a vacancy-abundant oxide support.

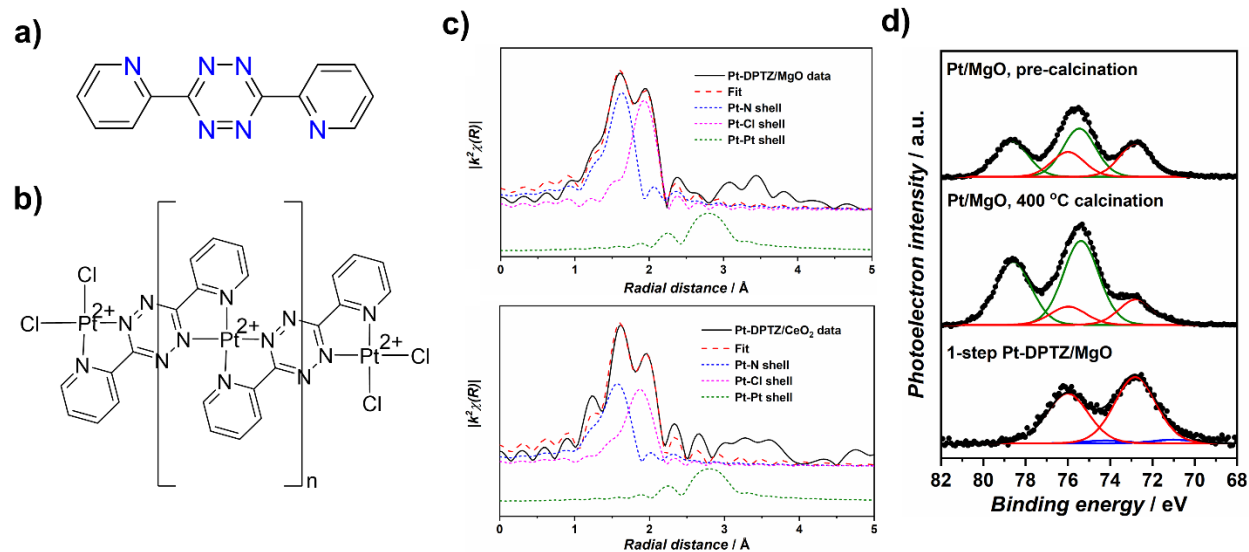


Figure 1. A summary of synthesis and characterizations of oxide-supported Pt-DPTZ SSCs: **(a)** the structure of DPTZ. **(b)** Proposed structure of Pt-DPTZ single-site complex chains on oxide supports, with Pt binding with surface O from the bottom or at chain ends are omitted. **(c)** First-shell EXAFS fittings of Pt-DPTZ/MgO (top) and Pt-DPTZ/CeO₂ (bottom) showing the absence of Pt–Pt shell. **(d)** Pt 4f XPS fittings showing on Pt-DPTZ/MgO, almost all Pt sites are of +2 oxidation states, with little metallic Pt(0) nanoparticles or mixed Pt(IV) oxide (Mg₂PtO₄) formation. Reprinted from reference [25], with permission from Elsevier.

Table 1. Catalytic performance of Pt-DPTZ SSCs and other catalysts in the hydrosilylation reaction between 1-octene **8** and dimethoxymethyl silane **9**.

Entry	Catalyst	<i>T</i> (°C)	<i>t</i> (min)	Yield ¹ (%)	Pt concentration (ppm)	TON per Pt ² (× 10 ³)
1	Pt-DPTZ/MgO ³	75	120	95	10	cc
2	Pt-DPTZ/MgO ³	70	30	44	10	9.0
3	Pt(NP)/MgO	70	30	4	81	0.2
4	Mg ₂ PtO ₄ /MgO	70	30	47	87	1.1
5	Pt-DPTZ/CeO ₂ ³	70	30	91	16	cc
6	Pt-DPTZ/CeO ₂	60	20	51	16	6.5
7	Pt(NP)/CeO ₂	60	20	73	40	3.7
8	Pt-DPTZ/Al ₂ O ₃ ³	70	30	85	32	cc
9	Karstedt catalyst ³	70	30	86	16	cc
10	Speier catalyst ³	70	30	13	16	cc

All reactions were performed with 3 mmol **8**, 2.5 mmol **9**, and 1.5 mL toluene (solvent).

¹ Yield values reported here are GC-MS values based on **9** because excess **8** (1.2 eq) was used.

² TON per Pt values are presented to compare activity and only calculated if **9** was not completely converted (cc).

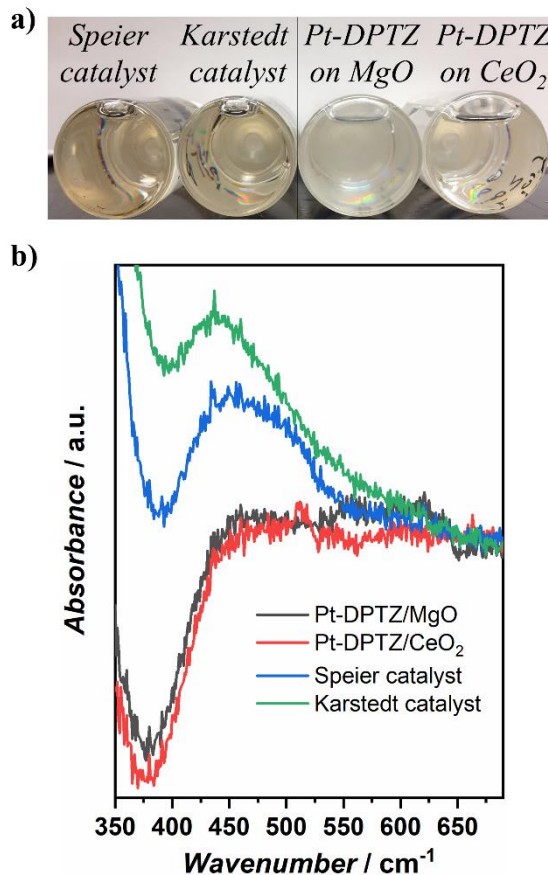
³ Data in these entries are reproduced from reference [25].

Table 1 shows that oxide-supported Pt-DPTZ SSCs are highly effective catalysts for the hydrosilylation reaction between 1-octene (**8**, Scheme 1) and dimethoxymethylsilane (**9**). Reactions were performed using 1.2 eq. of **8** due to unavoidable side reactions involving C=C bonds. C=C isomerization products 2-octene, 3-octene, and hydrogenation product octane were all identified by gas chromatography–mass spectrometry (GC-MS). 100% conversion of **9** was achieved with Pt-DPTZ SSCs under mild conditions (75 °C, 2 h on MgO, and 70 °C, 30 min on CeO₂ and Al₂O₃, entry 1, 5, and 8) at low Pt concentrations (< 35 ppm). GC yield of main

1
2
3
4 product **10** (calculated from **9**) is satisfactory (95% on MgO, 91% on CeO₂, and 85% on Al₂O₃),
5
6 and is comparable with or higher than both commercial homogeneous catalysts (86% on Karstedt
7
8 catalyst and 13% on Speier catalyst). Major Si-containing byproducts detected by GC-MS are
9
10 dimers **11** and **12**. The Performances of Pt-DPTZ SSCs are support-dependent, as it is less active
11
12 when supported on MgO than on CeO₂ or Al₂O₃ under same conditions (entry 2 compared with
13
14 entry 5 and 8). This partially originates from the lower Pt loading on MgO (0.09 wt% compared
15
16 with 0.35 wt% on CeO₂ and 0.7 wt% on Al₂O₃). Nevertheless, the turnover number per Pt value
17
18 (TON per Pt) on Pt-DPTZ/MgO at 70 °C in 30 min (9×10^3 , entry 2) is only approximately 1.5
19
20 times of that on Pt-DPTZ/CeO₂ at 60 °C in 20 min (6.5×10^3 , entry 6), indicating that activity
21
22 per Pt site is also affected by metal-support interactions. Average TOF values calculated from
23
24 TON per Pt (5.0 s^{-1} for entry 2 and 5.1 s^{-1} for entry 6) are significantly higher than previously
25
26 reported values on other Pt SSCs, Pt^{δ+}/TiO₂ ($< 0.21 \text{ s}^{-1}$ at 90 °C) and Pt/graphene (0.5 s^{-1} at
27
28 60 °C),^[19] showing the superiority of our Pt-DPTZ system. We note that metallic Pt NP are
29
30 almost catalytically inactive when supported on MgO (entry 3). CeO₂-supported Pt NP do exhibit
31
32 activity, but the TON per Pt is lower than that on Pt-DPTZ/CeO₂ SSC (3.8×10^3 in entry 7
33
34 compared with 6.5×10^3 in entry 6) with the same reaction time. Similarly, Mg₂PtO₄/MgO (the
35
36 stable bulk mixed oxide phase obtained after depositing Pt solely onto MgO and calcination
37
38 under air, entry 4) is active, but with a lower TON per Pt than Pt-DPTZ/MgO SSC (entry 2).
39
40 This is possibly due to one crucial advantage SSCs have over traditional metal aggregate
41
42 catalysts: the fraction of active metal centers is higher due to complete site isolation and uniform
43
44 chemical environments. The sharply contrasting activity between MgO and CeO₂-supported
45
46 Pt(0) NP again highlights impacts of metal-support interaction in this reaction, and reveals the
47
48
49
50
51
52
53
54
55
56
57
58
59
60
61
62
63
64
65

1
2
3
4 complexity behind the unsolved controversy in existing literature about whether colloidal Pt(0)
5
6 are active in this reaction or not.^[3a, 14-15]
7
8
9

10
11
12
13 **2. Comparison of Pt SSCs with commercial catalysts.** (a) *Selectivity.* As hydrosilylation
14
15 catalysts, Pt-DPTZ SSCs at surfaces show several advantages over commercial homogeneous
16
17 catalysts (Karstedt and Speier). The heterogeneous nature of SSCs at surfaces is a preferred
18
19 characteristic due to its easy separation, especially in small molecule synthesis. This advantage
20
21 of heterogeneous catalysts is usually accompanied by relatively low selectivity due to non-
22
23 uniform chemical environments of metal sites. Nonetheless, this trade-off is avoided in this
24
25 system, as higher selectivity and yield were achieved on Pt-DPTZ/MgO SSC (95%, entry 1 in
26
27 Table 1) than Karstedt catalyst (86%, entry 9). On Pt-DPTZ/MgO, the selectivity benefits from
28
29 the uniform structure of Pt sites, a unique feature of SSCs among heterogeneous catalysts. MgO
30
31 surfaces may also have geometric restrictions on the adsorption and reaction of substrates on Pt
32
33 sites, limiting undesired reaction pathways. On CeO₂ and Al₂O₃, the selectivity is slightly lower
34
35 (91% in entry 5 and 85% in entry 8), potentially due to the co-existence of multiple types of Pt
36
37 single-sites (such as PtO_xCl_y) at surface vacancies, but it is still at least comparable with Karstedt
38
39 catalyst. We note that the 86% yield on Karstedt catalyst reported here is close to and slightly
40
41 higher than previous literature reports (78%) under almost identical conditions,^[13a, 13b] so it is a
42
43 reliable reference. The heterogeneous nature of Pt-DPTZ SSCs also helps the selectivity by
44
45 exempting the use of a co-solvent. On Speier catalyst, the low yield (13% in entry 10) is due to
46
47 the exchange between methoxy groups in **9** or **10** and the co-solvent isopropanol, which does not
48
49 exist when using Pt-DPTZ SSCs. We recognize that the 13% yield can be improved by using less
50
51 isopropanol in catalyst preparation, but these side reactions are unavoidable.^[9, 27]
52
53
54
55
56
57
58
59
60
61
62
63
64
65



36 **Figure 2.** (a) A noticeable color difference between solutions of commercial Pt catalysts (left) and metal-ligand SSCs (right) indicates significantly less colloidal Pt formation for Pt-DPTZ SSCs than commercial Pt catalysts. From left to right: Speier catalyst, Karstedt catalyst, Pt-DPTZ/MgO, Pt-DPTZ/CeO₂. (b) UV-Vis spectra of post-reaction solutions exhibiting the 450-500 cm⁻¹ absorption with commercial catalysts but not with SSCs. Absorption of toluene was subtracted from the raw spectra.

37
38
39
40
41
42
43
44
45
46
47 (b) *Colloidal Pt formation.* One major drawback from which the Karstedt catalyst suffers is
48 the formation of colloidal Pt during the reaction, which is believed to cause side reactions and
49 long-term deactivation.^[3a, 15] Solutions were reported to gradually become yellow during the
50 reaction,^[13d, 28] and small Pt clusters were observed by microscopy after the reaction.^[15a, 29] This
51 problem is much less severe with Pt-DPTZ SSCs than commercial catalysts. A photo of post-
52 reaction solutions using Pt-DPTZ/MgO, Pt-DPTZ/CeO₂, Speier catalyst, and Karstedt catalyst of
53
54
55
56
57
58
59
60
61
62
63
64
65

1
2
3
4 the same Pt concentration is exhibited in Figure 2a. Solutions with both SSCs show significantly
5
6 lighter yellow color than two commercial catalysts. The color observation is confirmed by UV-
7
8 Vis spectra (Figure 2b), where solutions with both commercial catalysts have absorbance
9
10 between 450 and 500 cm^{-1} , consistent with the yellow color. In contrast, solutions with Pt-DPTZ
11
12 SSCs have negligible absorbance in this region, indicating less colloidal Pt formation. The four
13
14 post-reaction solutions were centrifuged to collect any solid product and imaged by transmission
15
16 electronic microscopy (TEM). SSC samples show smaller particles compared with large Pt black
17
18 bulk formed from the commercial catalysts (Figure S3). Meanwhile, XPS and XAS on post-
19
20 reaction Pt-DPTZ/SSCs show that Pt aggregation does not occur on surfaces (see next section),
21
22 *i.e.*, there is no Pt aggregation on the surfaces during the reaction. During SSC-catalyzed
23
24 reactions, only a fraction of Pt are leached into solutions (see next section), so the concentration
25
26 of Pt vulnerable to aggregation is lower than commercial catalysts that are homogeneous.
27
28 Furthermore, Pt leached off supports should also be more resistant to aggregation than Pt in
29
30 commercial catalysts, as the favorable N binding pockets and oxidizing ability provided by
31
32 DPTZ stabilize Pt(II) cations. In comparison, all ligands in Speier and Karstedt catalysts bind
33
34 with Pt relatively weakly and do not offer sufficient oxidizing potential to prevent the reduction
35
36 of Pt (the Karstedt catalyst consists of zero valent Pt). Consequently, Pt(0) colloids are formed
37
38 easily.
39
40
41
42
43
44
45
46
47
48
49
50
51
52
53
54
55
56
57
58
59
60
61
62
63
64
65

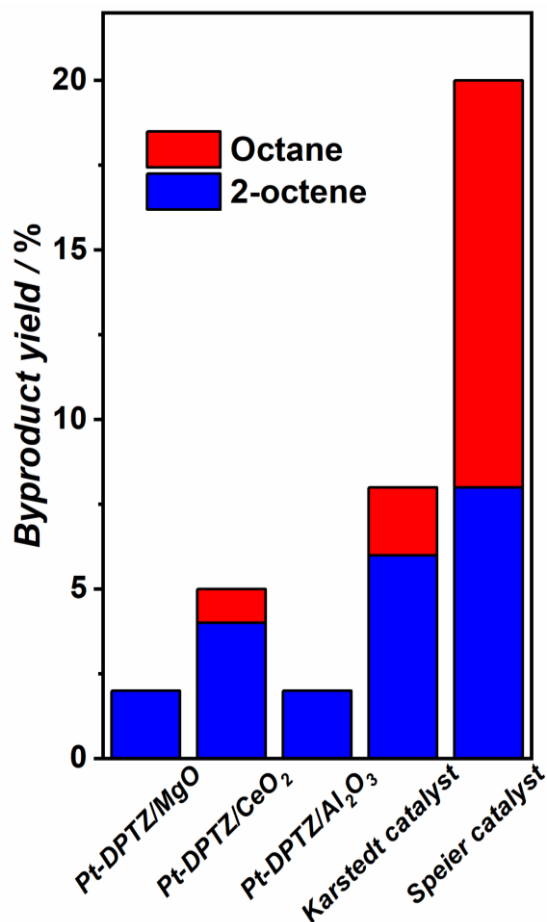
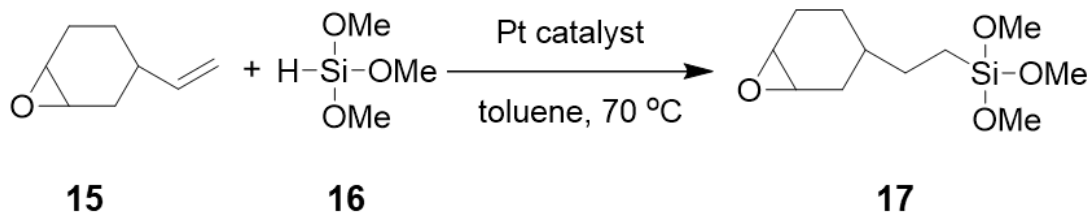


Figure 3. Comparison of byproducts yield from **8**, with blue bars showing isomerization product 2-octene yield, while red bars showing hydrogenation product octane yield.

(c) *Alkene isomerization and hydrogenation.* Two major side reactions in alkene hydrosilylation are isomerization and hydrogenation of the C=C bond, forming 2-octene/3-octene and octane from 1-octene (**8**), respectively. Figure 3 shows the yield of 2-octene and octane from **8** on Pt-DPTZ SSCs and commercial catalysts. These side reactions occur to a less extent on all Pt-DPTZ SSCs. Pt-DPTZ/CeO₂ generates the most byproducts among the three probably because of the abundant PtO_xCl_y single-sites at surface vacancies. We suspect that on Pt-DPTZ SSCs, the isomerization is a branch from the hydrosilylation cycle. First, we discovered that **8** alone, without the presence of **9**, cannot be isomerized or hydrogenated, with or without

1
2
3
4 colloidal Pt formed in hydrosilylation reaction. Besides, Figure S4 exhibits concentrations of 2-
5
6
7 octene and 3-octene detected at various reaction times normalized to their post-reaction
8
9 concentrations. The comparison of these two curves with the same curve for hydrosilylation
10
11 product **10** reveals that time scales of isomerization and hydrosilylation are similar. After
12
13 hydrosilylation stops due to the complete consumption of **9**, isomerization stops as well, despite
14
15 an excess of **8** in solution. These observations are similar with results reported by Kuhn et al. on
16
17 Karstedt catalyst,^[15b] where they claimed that isomerization results from the migratory insertion
18
19 step of the Chalk-Harrod hydrosilylation cycle (Figure S1), and its competition with
20
21 hydrosilylation is determined by which carbon binds with Pt after the insertion. Although
22
23 reaction mechanisms on Pt-DPTZ SSCs might differ from Karstedt catalyst, our observations
24
25 imply the same conclusion: hydrosilylation and isomerization likely branch from the same
26
27 catalytic cycle. Furthermore, some previous studies on Karstedt catalyst argued that colloidal Pt
28
29 formed during the reaction, not the Pt complex, are mainly responsible for isomerization.^[14a]
30
31 Nevertheless, our results suggest this is not the case for Pt-DPTZ SSCs. If colloidal Pt were
32
33 much more active in isomerization than Pt complexes, the byproduct formation would have been
34
35 very slow relative to the formation of **10** at the initial stage due to a lack of colloidal Pt, and
36
37 would accelerate as Pt aggregate gradually. However, in Figure S4, shapes of 2-octene and 3-
38
39 octene curves are highly similar with that of the **10** curve, contradicting this theory. Our results
40
41 suggest that isomerization and hydrosilylation mostly share the same active sites. Consequently,
42
43 less byproduct formation on Pt-DPTZ SSCs cannot be explained by less colloidal Pt formation
44
45 shown above. Instead, it may be relevant with the presence of support surfaces making
46
47 intermediates of side reactions less favorable electronically or sterically.
48
49
50
51
52
53
54
55
56
57
58
59
60
61
62
63
64
65



Scheme 2. Hydrosilylation reaction between 4-vinyl-1-cyclohexane 1,2-epoxide (**15**) and trimethoxysilane (**16**). Reaction conditions: 80 °C, 1 min, 16 ppm Pt, 2.5 mmol **16**, 3 mmol **15**, and 1.5 mL toluene as solvent.

(d) *Tolerance with epoxy group.* Another advantage of Pt-DPTZ SSCs over commercial catalysts is their tolerance towards the epoxy group in substrates. Hydrosilylation with epoxy-containing substrates is particularly important in Si-polymer industry because the epoxy group provides desirable physiochemical properties to products.^[2d, 30] Unfortunately, Karstedt catalyst has been known to show low selectivity in these reactions, as it catalyzes undesired ring-opening side reactions.^[13a, 13b] Our experiments show similar results: a 52% yield of desired product (**17**, Scheme 2) in the reaction involving epoxy-containing alkene (**15**) at 100% silane (**16**) conversion. This number is also consistent with previous reports (< 50%).^[13a, 13b] No major byproducts from ring-opening reactions were detected by GC-MS, so we suspect that reactants go through ring-opening polymerization, as suggested in prior studies.^[31] The yield of **17** further drops to 17% when no solvent was used, supporting the idea that main side reactions are intermolecular. Pt-DPTZ SSCs show obvious improvement over Karstedt catalyst regarding this problem: 71%, 64%, and 60% **17** yields were achieved when supported on CeO₂, Al₂O₃, and MgO, respectively. The electronic and geometric modifications provided by supports likely suppress side reactions in these cases, although this may not necessarily be true for other substrates. As with commercial catalysts and most other homogeneous catalysts,^[3a, 3b, 15b, 32] SSCs do not show any hydrosilylation activity when internal alkenes such as 2-octene are used.

1
2
3
4 **3. Evolution of Pt sites during catalysis.** (a) *Stability of Pt single-sites.* We examined the
5 stability and recyclability of Pt-DPTZ SSCs. Table 2 shows characterization results of MgO- and
6 CeO₂-supported Pt-DPTZ SSCs before and after catalysis (with 100% **9** conversion). Both SSCs
7 suffer from Pt leaching, which is less severe on CeO₂ (32%) than MgO (67%). The leaching was
8 confirmed by the presence of Pt in post-reaction solutions measured by inductively coupled
9 plasma mass spectrometry (ICP-MS). Nonetheless, the average TON on each Pt site during the
10 reaction is around 8000, so the leaching probability during one turnover cycle is small. Stirring
11 Pt-DPTZ/MgO in pure solvent (toluene) at reaction temperature without **8** or **9** led to 50% Pt
12 leaching, indicating that the natural solvent-thermal instability of Pt-DPTZ single-sites, instead
13 of hydrosilylation turnovers, accounts for most of the leaching from the MgO support. No
14 significant binding of DPTZ to these supports is observed without Pt,^[25] thus, the main attractive
15 force to hold Pt-DPTZ complexes on surfaces are Pt-support interactions.^[25] Therefore, the
16 difference in Pt stability on CeO₂ and MgO supports reflects a difference in the strength of Pt-
17 support interactions, which has been known to be stronger on CeO₂. Pt-DPTZ/Al₂O₃ was also
18 evaluated, which shows 50% Pt leaching after catalysis. We will focus on CeO₂ and MgO
19 supports in the following experiments to look at two extremes: CeO₂ offers the best Pt stability
20 and Pt leached from MgO is the most concentrated and best for analysis. Despite leaching,
21 Figure 4 shows that Pt-DPTZ/CeO₂ can be recycled four times with high yield of **10**, after which
22 the yield decreases gradually.
23
24
25
26
27
28
29
30
31
32
33
34
35
36
37
38
39
40
41
42
43
44
45
46
47
48
49
50
51
52
53
54
55
56
57
58
59
60
61
62
63
64
65

Table 2. XPS analysis of MgO- and CeO₂-supported Pt-DPTZ SSC before and after hydrosilylation catalysis.

	Pt-DPTZ/CeO ₂		Pt-DPTZ/MgO	
	Fresh	Used	Fresh	Used
Pt loading (wt%) ¹	0.35	0.24	0.09	0.03
Pt 4f _{2/7} binding energy (eV)	72.7	72.8	72.8	72.6
Pt(II) fraction ²	> 0.9	0.9	0.9	0.7
Pt(0) fraction	< 0.1	0.1	0.1	0.3
DPTZ : Pt ³	0.47	0.47	0.73	0.75
Cl : Pt ³	0.98	0.55	0.92	1.01

¹ Pt loading values were calculated from ICP-MS measurements.

² Pt(IV) have not been observed with meaningful quantity on any samples.

³ DPTZ : Pt (or Cl : Pt) ratios were calculated using XPS peak area of N 1s (or Cl 2p) region and Pt 4f region.

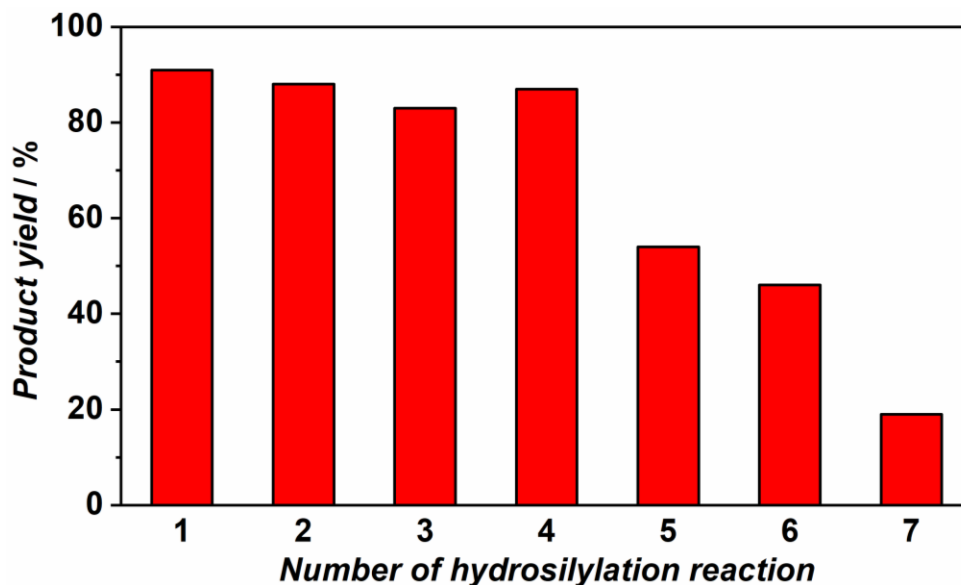


Figure 4. Recyclability test of Pt-DPTZ/CeO₂ SSC. Reaction conditions: 70 °C, 20 min, 15 mg catalyst. After each run, solid catalysts were separated from the solution by centrifuge and reused in the next.

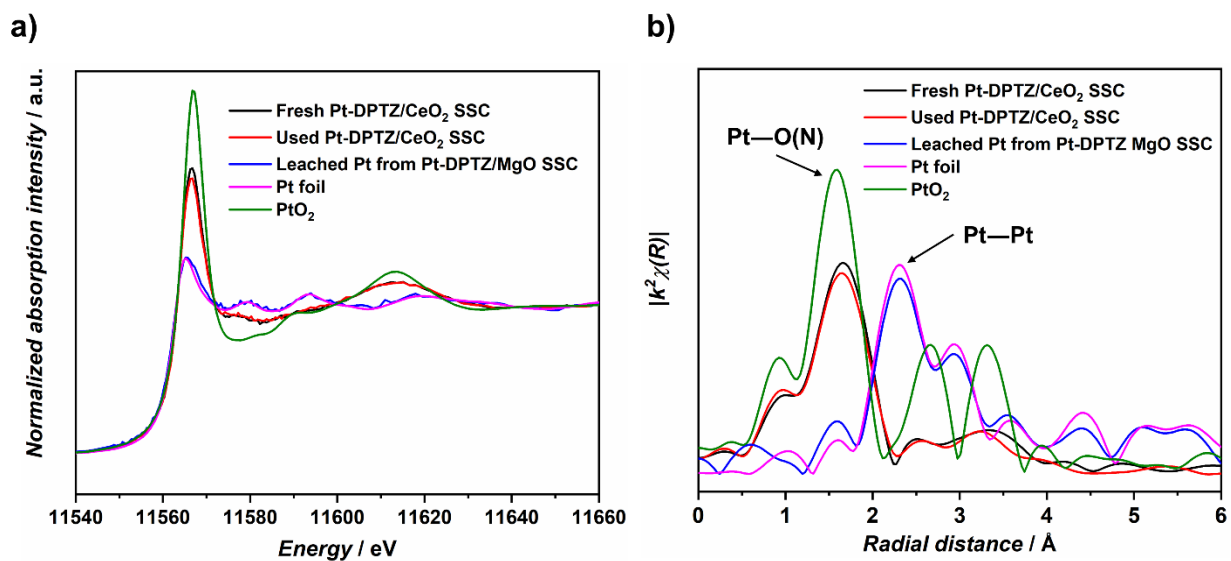


Figure 5. Pt *L*₃-edge XAS of fresh (black) and used (red) Pt-DPTZ/CeO₂ SSC, Pt leached during catalysis from Pt-DPTZ/MgO SSC (blue), Pt foil standard (purple), and PtO₂ standard (green). (a) XANES region after normalization. (b) Fourier transform magnitudes of EXAFS region in *R*-space.

The structure of Pt sites after catalysis was revealed by XAS and XPS. *R*-space EXAFS (Figure 5b) at the Pt *L*₃ edge of post-reaction Pt-DPTZ/CeO₂ SSC (red) exhibits similar features with its fresh form (black). A Pt—Pt shell is not observed, proving that recycled CeO₂-supported Pt retain their single-site character after catalysis. As shown in our prior work, all first-shell intensities in the fresh catalyst are fit well by contributions from the Pt—O(N) shell (~1.6 Å) and the Pt—Cl shell (~1.9 Å).^[25] XPS data indicate a decrease in Cl concentration after the reaction, but there is not a noticeable change in EXAFS data (Figure 5b, red), which may be due to the formation of Pt—Si (~1.85 Å) or Pt—C bonds (with C=C π coordination, ~1.75 Å) after the loss of Cl. Close examination of the Pt *L*₃ X-ray absorption near edge structure (XANES) region (Figure 5a) reveals that the white line intensity does not change significantly before and after reaction. White line intensity in normalized XANES spectra often positively correlates with metal oxidation states because it represents transitions from core orbitals to unfilled valence

1
2
3
4 orbitals. In this case, the white line intensity remains between that of Pt foil (purple curve) and
5
6 PtO₂ (green curve) standards, indicating that the Pt oxidation state is between 0 and +4. Previous
7
8 XPS results show Pt exist as Pt(II) single-sites before catalysis,^[25] so the Pt oxidation state
9
10 remains close to +2 after catalysis. We also performed XAS on post-reaction solution containing
11
12 Pt leached from Pt-DPTZ/MgO (Figure 5b, blue), to verify the formation of colloidal Pt in
13
14 solution suggested by the yellow color (Figure 2a) and TEM images (Figure S3). We note that in
15
16 the case of Pt-DPTZ/CeO₂, the amount of leached Pt is too small to analyze by XAS. As
17
18 expected, Pt leached from Pt-DPTZ/MgO shows a strong Pt—Pt shell and a white line intensity
19
20 close to Pt foil, consistent with Pt(0) colloids. Other scattering paths from adsorbates on colloidal
21
22 Pt or from soluble Pt single-sites are too weak compared with the Pt—Pt shell to be detected by
23
24 EXAFS, suggesting that the vast majority of leached Pt exists in relatively large Pt colloids.
25
26 These results prove that Pt aggregation does occur, but exclusively in solution, not on supports.
27
28 These conclusions are further supported by XPS results in Table 2. Compared with fresh
29
30 catalysts, Pt 4f_{2/7} binding energy of Pt-DPTZ SSCs does not change significantly after catalysis,
31
32 and most Pt still exist in +2 oxidation states (peak fittings results see Figure S5). We note that on
33
34 MgO, although the fraction of Pt(0) appears to increase after the reaction (Figure S5a), the
35
36 amount of Pt(0) stays almost constant after considering the decrease of total Pt content. The
37
38 apparent increase in Pt(0) fraction is simply a result of Pt(II) leaching. The DPTZ : Pt ratio on
39
40 used catalysts is similar with that on fresh ones, implying the coordination between DPTZ and Pt
41
42 does not change significantly either. A decrease in Cl : Pt ratio was observed on CeO₂, as some
43
44 Cl might leave Pt during the reaction and then be replaced by reactants and/or products.
45
46
47
48
49
50
51
52
53
54
55
56
57
58
59
60
61
62
63
64
65

1
2
3
4 (b) *Active species: single-sites or colloids?* Considering the non-negligible Pt leaching and Pt
5
6 aggregation in solution, it is necessary to question whether it is the colloidal Pt that is the
7
8 catalytically active Pt species. The same question has been discussed on Karstedt catalyst in
9
10 previous literature.^[13d, 15, 28-29] Earlier studies supported colloidal Pt as active species,^[28b, 29] but
11
12 most recent work rejected this theory.^[15] Our work also indicates that the colloidal Pt is not the
13
14 main active species in our Pt-DPTZ SSC systems.
15
16
17
18

19
20 After a reaction that converted **9** completely (70 °C for 30 min or 75 °C for 2 h when
21
22 supported by CeO₂ or MgO, respectively), the solution/solid mixture was centrifuged at a speed
23
24 that keeps all colloidal Pt in the solution (details in SI). The separated solid and solution were
25
26 then each used as catalysts in separate experiments to conduct a second reaction at the same
27
28 temperature, but for much shorter time (3 min on CeO₂ or 30 min on MgO). Table 3 shows that a
29
30 17% yield was achieved on recycled Pt-DPTZ/CeO₂, compared with only 4% on the colloidal Pt
31
32 in solution. For comparison, fresh Pt-DPTZ/CeO₂ yielded 19% **10** in the first 3 min. Note that in
33
34 the first 3 min reaction with fresh catalyst, the concentration of colloidal Pt is much lower than
35
36 that in the post-reaction solution because they form gradually as the reaction proceeds.
37
38

39
40 Therefore, turnovers on colloidal Pt in this 3 min should be responsible for significantly less than
41
42 4% **10** yield, which is only 1/5 of the 19% total **10** yield. We conclude that despite the possibility
43
44 that colloidal Pt might be an active hydrosilylation catalyst, most turnovers occur on Pt single-
45
46 sites. When TON per Pt values are used for comparison, it is also clear that colloidal Pt are much
47
48 less active in the first 3 min (1.5×10^3) than Pt single-sites (2.4×10^3 in the first run and $3.2 \times$
49
50 10^3 in the second). On MgO, despite more severe Pt leaching and less active Pt single-sites, Pt
51
52 single-sites still show higher activity per Pt in the second run (TON per Pt = 13.0×10^3) than
53
54 colloidal Pt (9.5×10^3). We note that, despite the indication by EXAFS that in post-reaction
55
56
57
58
59
60
61
62
63
64
65

solutions (after removing the solid material) most Pt exist as colloidal Pt, we cannot eliminate the presence of soluble Pt single-sites, which may contribute to the turnovers.

Table 3. Performances of CeO₂- and MgO-supported Pt-DPTZ SSCs at various state.

Support	Reaction condition	Catalyst state	Yield (%)	TON per Pt ($\times 10^3$)
CeO ₂	70 °C, 3 min	Fresh	19	2.4
		Recycled ¹	17	3.2
		Post-reaction solution ¹	4	1.5
		Fresh, pre-treated by 1-octene ²	38	4.8
MgO	75 °C, 30 min	Fresh	44	9.0
		Recycled ¹	21	13.0
		Post-reaction solution ¹	31	9.5

All reaction were performed with 3 mmol **8**, 2.5 mmol **9**, and 1.5 mL toluene as solvent. MgO reactions were performed with 25 mg catalyst; CeO₂ reactions were performed with 15 mg catalyst.

¹ The first reaction before these reactions were performed at 70 °C, 30 min (CeO₂) or at 75 °C, 2 h (MgO). After the reaction, solid and solution were separated by centrifuge.

² Pretreatments with 1-octene were conducted at the reaction temperature for 30 min.

(c) *Structure of Pt at different stages of hydrosilylation.* The results above indicate that Pt single-sites are the main active species and that they remain isolated on these surfaces after catalysis. However, the most active form of Pt seems to be different from the ideal structure shown in Figure 1b because of the induction period observed on Pt-DPTZ/CeO₂. Figure 6 presents the yield of **10** with reaction time on Pt-DPTZ/CeO₂, showing a clear acceleration during the first 3 min. Reaction rate then drops due to the consumption of reactants. Previous studies on Karstedt and Speier catalyst also reported induction periods, which some attribute to ligand exchange processes.^[9-10, 15b] On both supports, the recycled Pt-DPTZ SSCs exhibit higher

TONs per Pt in the corresponding reaction time (3.2×10^3 on CeO₂, 13.0×10^3 on MgO) than fresh ones (2.4×10^3 on CeO₂, 9.0×10^3 on MgO). This also indicates the presence of an induction period: the recycled catalyst has been activated during the first run and thus catalyzes more turnovers in the second run during the initial stage of the reaction.

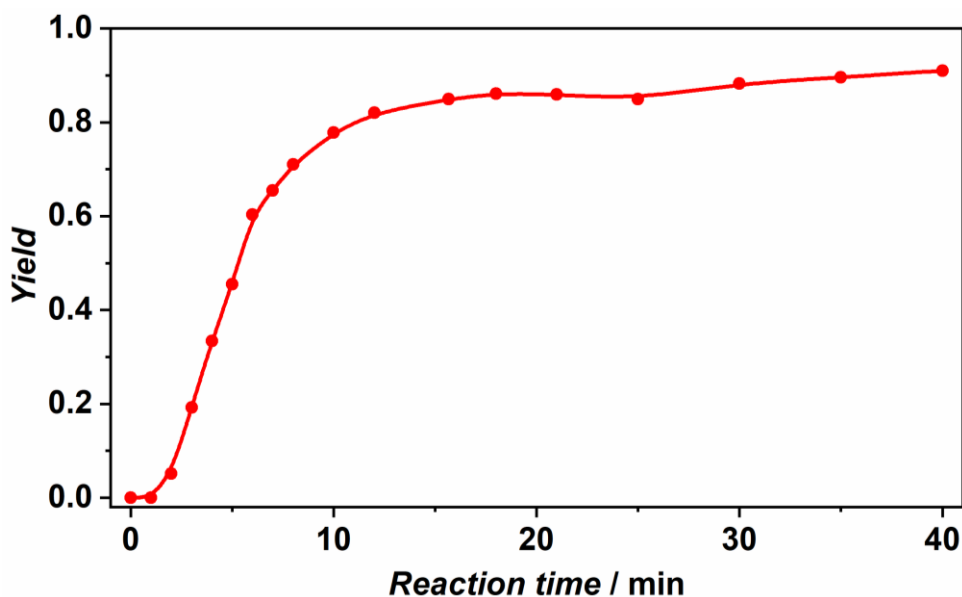


Figure 6. Yield of hydrosilylation product **10** with reaction time on Pt-DPTZ/CeO₂ SSC. The acceleration in reaction rate at the beginning indicates an induction period. The differential form of this figure, showing the rate vs. time is presented as Figure S6.

Since colloidal Pt are less active than Pt single-sites, the induction period cannot be explained by the formation of colloidal Pt. Previous reports linked the induction period on the Karstedt catalyst with the coordination of Pt sites with reactant alkene.^[15] We found that pre-treating Pt-DPTZ/CeO₂ SSC with 1-octene at the reaction temperature before the reaction enhances the initial activity of Pt-DPTZ/CeO₂ by a factor of 2 (Table 3, with a yield increase from 19% to 38% in the first 3 min, and a TON per Pt increase from 2.4×10^3 to 4.8×10^3). In contrast, pretreatments with hydrosilylation-resistant 2-octene or reactant silane **9** do not have

1
2
3
4 this effect. We also noticed that with Pt-DPTZ/CeO₂, the Cl : Pt ratio drops by half after catalysis
5
6 (Table 2), implying Cl detachment from Pt during catalysis. This is intuitive as Cl atoms are
7
8 typically regarded as good leaving groups in organometallic chemistry.
9

10
11 We also performed *in situ* XAS to further investigate the structure of active sites. The
12
13 reaction was performed under the same condition as Figure 6, but quenched at 1, 2, 5, and 10
14
15 min by placing the reaction tube into a dry ice bath, allowing us to detect the chemical
16
17 environment of Pt at various stages of the reaction by XAS. In these experiments, Pt
18
19 coordination environments are complicated by the presence of Pt–Si and Pt–C bonds from
20
21 intermediates and the spectra quality is limited by the extremely low Pt concentration in the
22
23 reaction mixture (~10-20 ppm), so a rigorous quantitative fitting with multiple shells is not
24
25 possible, but we analyze these qualitatively. Figure 7a shows that after 2 min reaction, when the
26
27 induction period is almost complete (according to Figure 6 and S6), the intensity at ~1.9 Å
28
29 (Pt–Cl) drops, and the first-shell peak shifts to shorter distance compared with fresh catalyst.
30
31 This is consistent with the loss of Pt–Cl coordination from XPS results. Figure 7a also shows
32
33 that similar changes occur during the 1-octene pre-treatment, indicating that the shorter induction
34
35 period due to pre-treatment is also due to Cl loss.
36
37
38
39
40
41
42
43
44
45
46
47
48
49
50
51
52
53
54
55
56
57
58
59
60
61
62
63
64
65

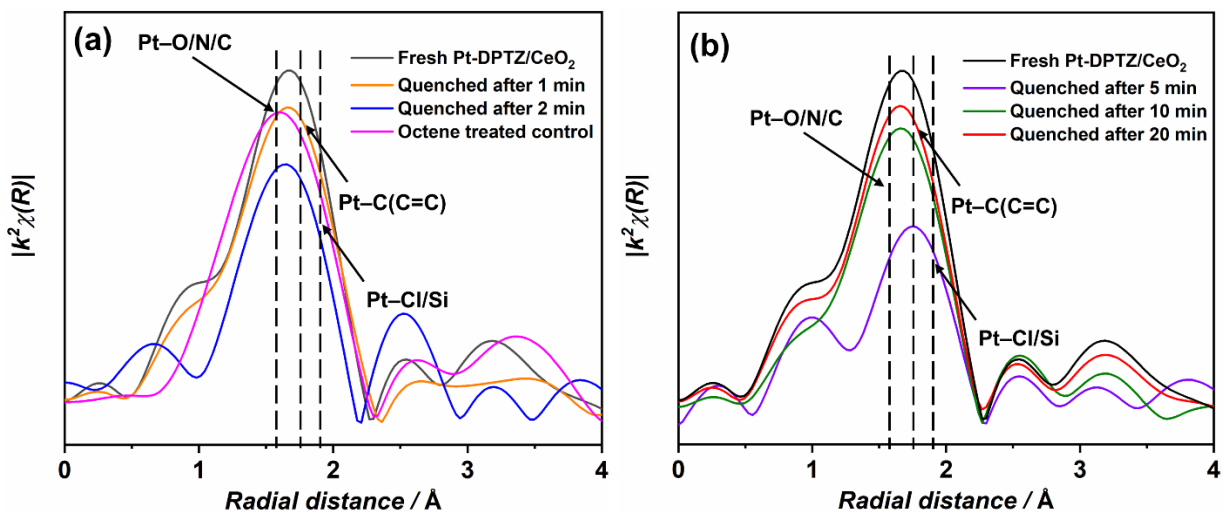


Figure 7. Pt L_{3} -edge XAS (EXAFS region in R -space, k^2 -weighted) of Pt-DPTZ/CeO₂ SSC at various stages of the hydrosilylation reaction. Panel (a) shows fresh (black), quenched after 1 min (orange) and 2 min (blue) of reaction, and collected *in situ* (70 °C) under 1-octene treatment. Panel (b) shows fresh (black) and quenched after 5 min (purple), 10 min (green), and 20 min (red) of reaction. At 20 min, the reaction has run to completion.

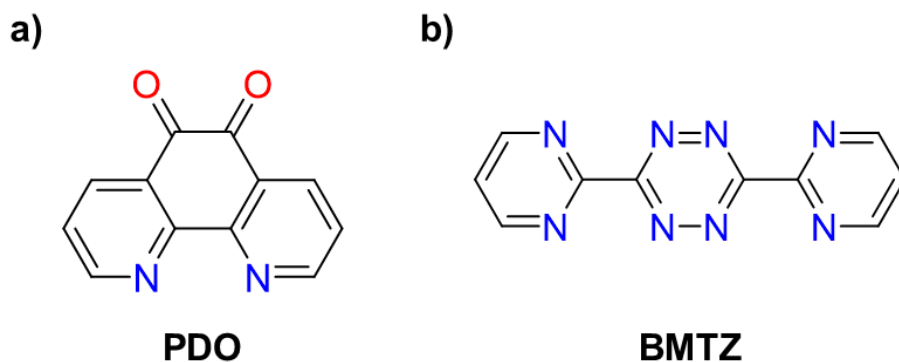
Figure 7b compares the coordination environment of Pt when the turnover is fastest (5 min) and when the reaction is close to complete (10 min) with catalyst at the end of the reaction (20 min). EXAFS after 5 min reaction (purple) has a first-shell peak around 1.76 Å with significantly lower intensity than fresh catalyst, especially at ~1.6 Å. Considering the loss of Pt—Cl coordination during catalysis, this suggests more contribution from Pt—Si (~1.85 Å) and Pt—C π (~1.75 Å) bonds than Pt—O/N bonds (~1.6 Å). This is in sharp contrast with spectra from fresh catalyst (black curve) where the first-shell peak was located at 1.65 Å, which is from the combination of Pt—O/N bonds and Pt—Cl (~1.9 Å) bond. The peak position shift and intensity drop at 5 min indicate that after the induction period, the most active Pt species have less O and N coordination, implying that they are detached from DPTZ and CeO₂. As reaction completes

1
2
3
4 (10 min and 20 min, green and red, respectively), the first-shell peak shifts back toward 1.65 Å,
5
6 suggesting the detachment is reversible. XPS on solid catalyst obtained from quenching after 5
7
8 min show a decrease in Pt content to 50% of its fresh form. However, after 30 min of reaction,
9
10 68% of the original Pt content is found on the solid catalyst. The DPTZ : Pt ratio is virtually
11
12 unchanged in both of these measurements compared to fresh catalyst (Table 2), indicating that
13
14 the reattachment of Pt restores it to the supported metal-ligand state.
15
16
17
18

19
20 The detachment of Pt from ligand and/or support is not surprising. Previous EXAFS analysis
21
22 suggests that the coordination number of Pt on fresh SSCs is between 4 and 5.^[25] Even after Cl
23
24 leaves during the induction period, the Pt coordination shell is still crowded for the reaction to
25
26 proceed with Chalk-Harrod (Figure S1) or similar mechanisms. None of the quenching spectra
27
28 shown in Figure 7 have significant contribution from Pt–Pt bonds, so the formation of Pt colloids
29
30 is minimal with Pt-DPTZ/CeO₂ SSC. We note that after 5 min, the shift of the first shell away
31
32 from ~1.6 Å also suggests a low contribution of Pt–C σ bonds compared with Pt–Si or Pt–C π
33
34 bonds. This is significant because it implies that regardless of the exact mechanism, the rate-
35
36 determining step is not reductive elimination forming C–H bond (step III_{HS} in Figure S1).
37
38
39
40

41
42 Overall, our results depict a complicated picture of how Pt-DPTZ single-sites evolve during
43
44 hydrosilylation catalysis. The initial coordination of reactant alkene and leaving of Cl from Pt
45
46 complete the induction period. At the most active stage of the reaction, Pt single-sites likely
47
48 detach temporarily from DPTZ or support to provide necessary coordination vacancies. As the
49
50 reaction completes, most Pt are recovered by re-coordinating with DPTZ and support, with a
51
52 small fraction of Pt remaining in solution. On-surface Pt are still single-sites after catalysis, while
53
54 leached Pt aggregate into colloids that are less active than single-sites. Further details of the
55
56 reaction mechanisms are the subject of ongoing studies.
57
58
59
60
61
62
63
64
65

1
2
3
4
5
6
7
8 **4. Impact of ligand and support on Pt activity.** The impact of the ligand environment on
9
10 the activity of the metal center is an important aspect of organometallic catalysis. In order to
11
12 explore this aspect in our system, we replaced DPTZ with PDO and BMTZ ligands (Figures 8a,
13
14 8b) on both supports (CeO₂ and MgO). Both ligands have at least two binding pockets, allowing
15
16 the growth of Pt-ligand complexes similar with Pt-DPTZ. Table 4 shows that for all six Pt-ligand
17
18 SSCs, the binding energy of Pt 4f_{2/7} XPS peak does not deviate significantly from 72.8 eV,
19
20 suggesting that most Pt are Pt(II) single-sites. BMTZ has a stronger electron affinity (oxidizing
21
22 potential) than DPTZ and leads to the formation of +3 metal centers with V in model systems (on
23
24 single crystal metal supports in UHV),^[26c] but similar systems with Pt prefer a mixed redox
25
26 isomer of Pt(II)/Pt(0) over odd-electron Pt oxidation states.^[33] Here, it is interesting that
27
28 simultaneous impregnation of Pt and BMTZ onto CeO₂ and MgO powders generates mainly
29
30 Pt(II), similar to DPTZ, due to the difference in support interaction. On each of the supports
31
32 studied, we observed the trend that ligand:Pt and Cl:Pt ratios (XPS) are negatively correlated
33
34 with each other, where a higher ligand:Pt ratio implies longer chain length (larger *n* in Figure
35
36 1b).
37
38
39
40
41
42
43



59 **Figure 8.** Structures of other ligands used in this work: (a) 1,10-phenanthroline-4,7-ketone
60 (PDO). (b) Bis-pyrimidyltetrazine (BMTZ).
61
62
63
64
65

Table 4. Catalytic performances and XPS characterization results of Pt-ligand SSCs with various ligands on MgO and CeO₂.

Support	Ligand	Yield (%)	Pt loading (wt%)	TON per Pt ($\times 10^3$)	Pt 4f _{2/7} BE (eV)	Ligand : Pt	Cl : Pt
CeO ₂ (60 °C, 20min)	DPTZ	51	0.34	5.4	72.9	0.47	1.56
	BMTZ	19	0.33	1.6	72.9	0.67	1.31
	PDO	29	0.81	1.3	72.9	1.03	1.17
MgO (75 °C, 30min)	DPTZ	68	0.09	8.6	72.8	0.73	0.92
	BMTZ	0	0.21	0.0	72.9	0.93	0.43
	PDO	53	0.05	10.7	72.3	0.37	1.03

All reaction were performed with 3 mmol **8**, 2.5 mmol **9**, and 1.5 mL toluene as solvent. MgO reactions were performed with 25 mg catalyst; CeO₂ reactions were performed with 15 mg catalyst.

Table 4 shows that the activity of Pt single-sites is highly sensitive to the choice of ligand and support. On both supports, Pt single-sites are most active when binding with DPTZ. The choice of ligand could be important for several reasons. First, on the same support, the activity measured by TON per Pt is positively correlated with Cl : Pt ratio. It is possible that the end-of-chain Pt that bind with Cl are more active because Cl is a better leaving group than DPTZ or support. Second, the distribution of Pt sites between outer surfaces and mesopores of the support depends on the ligand (see SI for details), which might affect activity too. Nonetheless, these two factors alone cannot explain the ligand dependence completely, as in the extreme case of Pt-BMTZ/MgO, no activity was observed despite the presence of Cl-bound Pt and a relatively high Pt loading compared with other ligands on MgO. We propose this is because Pt activity in this reaction is known to be sensitive to electronic structure, which is modified by the ligand. In homogeneous catalysis, ligand tuning offers an effective strategy to steer activity/selectivity of

1
2
3
4 metal centers. Results here suggest that one can apply this powerful tool to metal-ligand SSCs.
5
6 This enables fine tuning electronic structures of metal centers, which is extremely difficult with
7
8 traditional supported metal catalysts. Table 4 also highlights impacts of support again, as Pt
9
10 activity also varies with the support when the same ligand is used. An oxide support is
11
12 effectively a “heterogeneous ligand” that alters the electronic structures of Pt sites in a similar
13
14 way with organic ligands; its surface structure also plays a role in determining the distribution of
15
16 Pt sites: vacancy-abundant CeO₂ prevents the long-range growth of Pt-DPTZ chains, creating
17
18 more end-of-chain sites and vacancy-trapped PtO_xCl_y sites. The porous structure of supports can
19
20 affect the location of Pt sites. These factors all contribute to the activity of Pt. We are currently
21
22 performing systematic investigation on support effects through defect engineering on oxide
23
24 surfaces.
25
26
27
28
29
30
31
32
33
34

35 **Conclusions**

36
37
38 In this work, oxide-supported Pt-ligand SSCs synthesized by metal-ligand self-assembly are
39
40 presented as highly effective heterogeneous catalysts for alkene hydrosilylation reactions. These
41
42 SSCs provide unique advantages by combining the easy separation/recovery of heterogeneous
43
44 catalysts with the high metal utilization efficiency/uniformity of homogeneous catalysts.
45
46 Compared with current commercial catalysts, SSCs offer several advantages in easier catalyst
47
48 recovery, improved selectivity, less colloidal Pt and alkene byproduct formation, as well as better
49
50 tolerance towards epoxy groups in substrates. We found that Pt single-sites are leached into
51
52 solution at a slow rate compared with reaction turnover. XAS and XPS show that leached Pt then
53
54 aggregate into colloidal Pt that are much less active, while supported Pt remains as single-sites.
55
56 Despite the leaching problem, Pt-DPTZ/CeO₂ SSC exhibits satisfactory recyclability. During the
57
58
59
60
61
62
63
64
65

1
2
3
4 induction period, the coordination of Pt with reactant alkene and leaving of Cl are likely required
5
6 to activate Pt. DPTZ and support might reversibly detach from Pt at the most active stage to
7
8 further provide coordination vacancies. We also discovered that the activity of Pt single-sites is
9
10 sensitive to the choice of ligand and support. This might originate from the tuning of the
11
12 electronic structure of Pt centers as well as the distribution of Pt on supports, and offers vast
13
14 potentials for the fine tuning of metal single-sites.
15
16
17
18
19
20

21 **Experimental section**

22
23 **Synthesis of supported Pt-ligand SSCs.** The impregnation synthesis procedure of Pt-ligand
24
25 SSCs has been described in detail in our previous publication.^[25] In short, oxide support and
26
27 H₂PtCl₆·6H₂O (Alfa Aesar, 99.95% metal basis) solution were added to the solution of a ligand
28
29 (3 eq. of Pt) sequentially. 1-butanol (Alfa Aesar, 99%), water, and acetone (VWR, ACS grade)
30
31 were used as the solvent for DPTZ (Sigma Aldrich, 96%), PDO (Sigma Aldrich, 98%), and
32
33 BMTZ (synthesized by Ken Caulton group at IU),^[26c, 34] respectively. The mixture was stirred
34
35 overnight and solvent was evaporated at room temperature under dry air flow. The powder
36
37 catalyst materials were washed with water then DCM until free of residual ligands.
38
39
40
41
42

43
44 **General procedures for alkene hydrosilylation reactions.** The Karstedt catalyst used in
45
46 this work was purchased from Sigma Aldrich (2% in xylene, diluted to 0.1% with toluene). The
47
48 Speier catalyst was prepared by dissolving H₂PtCl₆·6H₂O in isopropanol (Macron, ACS grade) to
49
50 make Pt concentration as 177 ppm. Pt catalysts (supported Pt SSCs or commercial catalysts)
51
52 were weighed and kept in an empty reaction tube with cap. 2.5 mmol silane **9** (Alfa Aesar, >
53
54 97%) or **16** (Sigma Aldrich, 98%, mixture of isomers) and 3 mmol alkene **8** (Alfa Aesar, > 97%)
55
56 or **15** (Sigma Aldrich, 98%) were weighed into another reaction tube, and 1.5 mL toluene
57
58
59
60
61
62
63
64
65

1
2
3
4 (Macron, ACS grade) was added to the same tube. Both tubes were pre-heated in a water bath at
5
6 the reaction temperature for 10 min, before reactants and solvent were added into the tube with
7
8 Pt catalysts. The tube was capped during the reaction to avoid evaporation of silane with low
9
10 boiling point. After the reaction, the tube was cooled down quickly with cold water flow, the
11
12 solid catalysts were filtered out, and the liquid mixture was diluted for GC-MS measurements
13
14 with an Agilent 6890N Gas Chromatograph and 5973 Inert Mass Selective Detector. Product
15
16 yields were calculated from their response intensity ($m/z = 203.2, 91.2, 83.2,$ and 85.2 for
17
18 product **10**, **17**, 2-octene, and octane respectively) in GC-MS with respect to the response of
19
20 internal standard decane (Sigma Aldrich, > 99%) at $m/z = 142.2$ using pre-made calibration
21
22 curves. All pure compounds for calibration curves were purchased from Sigma Aldrich. Use
23
24 solid catalysts were collected for further characterization. The experiment measuring product
25
26 yield at various reaction time was performed in a round-bottom flask with 10 times amount of
27
28 catalysts, reactants, and solvent. At each reaction time, around 0.2 mL reactant mixture was
29
30 taken out and shot into 10 mL toluene at room temperature immediately to ensure quick
31
32 temperature drop. GC-MS measurements were then performed on each sample to measure
33
34 product yields.
35
36
37
38
39
40
41
42
43

44 **Characterization of Pt-ligand SSCs.** XPS measurements were performed with a PHI
45
46 Versaprobe II XP spectrometer using a monochromated Al X-ray source. A small amount of
47
48 each powder sample was fixed onto a platen with double-sided tape. For CeO₂-supported
49
50 samples, XPS were collected at Pt *4f*, N *1s*, C *1s*, Cl *2p*, Ce *3d*, and O *1s* regions. For MgO-
51
52 supported samples, Mg *2s* region was measured instead of Ce *3d*. A neutralizer was used to
53
54 alleviate surface charging. The binding energy was corrected with C *1s* peak (284.8 eV) for
55
56
57
58
59
60
61
62
63
64
65

1
2
3
4 MgO-supported samples, and Ce $3d_{5/2}$ main peak (882.4 eV) for CeO₂-supported samples.
5
6

7 Details about XPS data processing are included in the SI.
8
9

10 Selected samples were characterized on JEOL JEM 1010 TEM which operated at 80 keV.
11
12 Additional characterization with STEM was completed with JEOL JEM 3200FS operating at 300
13
14 keV. The TEM and STEM samples were prepared by centrifuging the post-reaction solutions to
15
16 form a pellet from any solid product in the solutions. The collected solid was redispersed in a
17
18 minimal amount of acetone and dropcast onto the TEM grid.
19
20
21

22
23 XAS measurements were performed at the 9-BM beamline at the Advanced Photon Source
24
25 of Argonne National Laboratory. Solid samples were pressed into pellets with $d \approx 7$ mm and
26
27 solution samples were placed in a PEEK container with magnetic stirring to prevent Pt
28
29 precipitation. The monochromatized X-ray energy was calibrated with the $L3$ -edge of a Pt foil
30
31 (11562.6 eV). X-ray absorption spectra were measured at the Pt $L3$ -edge, from 11363 to
32
33 12365 eV. For solid samples, both fluorescence and transmission data were collected and
34
35 fluorescence data were used for analysis. For liquid samples, only fluorescence data were
36
37 collected. XAS of a Pt foil, an α -PtO₂ pellet, and a K₂PtCl₆ pellet were measured as standard
38
39 references; transmission data were used for analysis of standards. ICP-MS measurements were
40
41 performed at IU Department of Earth & Atmospheric Sciences with an Agilent 7700 quadrupole
42
43 ICP-MS instrument. Solid catalysts were treated with aqua regia to dissolve all Pt before
44
45 measurement. For solution samples, the solvent was evaporated first and then the residue was
46
47 treated with aqua regia to dissolve all Pt. UV-Vis spectra of post-reaction solutions were
48
49 collected at IU Physical Biochemistry Instrumentation Facility with a Varian Cary 100 Bio
50
51 UV/Visible Spectrometer. A cuvette was filled with each solution sample and toluene, and
52
53
54
55
56
57
58
59
60
61
62
63
64
65

1
2
3
4 spectra were collected from 250 to 700 cm^{-1} . Absorption from toluene was subtracted from each
5
6 spectrum to ensure the 600 – 700 cm^{-1} region is flat.
7
8
9

10 11 12 **Acknowledgement**

13
14
15
16 This work was supported by the U. S. Department of Energy, Office of Basic Energy Sciences,
17
18 Chemical Sciences program, DE-SC0016367. XPS measurements were carried out at Indiana
19
20 University (IU) Nanoscale Characterization Facility with assistance from Dr. Yaroslav Lasovj.
21
22 Access to XPS at the Nanoscale Characterization Facility was provided by the NSF Award DMR
23
24 MRI-1126394. Transmission electron microscopy (TEM) imaging was performed at the IU
25
26 Electron Microscopy Center. XAS measurements were performed at beamline 9-BM at the
27
28 Advanced Photon Source, a U. S. DOE Office of Science User Facility operated for the DOE
29
30 Office of Science by Argonne National Laboratory under Contract No. DE-AC02-06CH11357.
31
32 Dr. Xuemei Zhou assisted with XAS measurements. GC-MS measurements were carried out at
33
34 the IU Mass Spectrometry Facility with assistance from Dr. Jonathan A. Karty.
35
36
37
38
39
40
41
42
43

44 **Conflicts of interest**

45
46
47 There are no conflicts of interest to declare.
48
49
50
51
52
53

54 **Keywords:** heterogeneous catalysis, single-site catalyst, hydrosilylation, platinum, X-ray
55
56 photoelectron spectroscopy, X-ray absorption spectroscopy
57
58
59
60
61
62
63
64
65

References

- [1] L. Sommer, E. Pietrusza, F. Whitmore, *J. Am. Chem. Soc.* **1947**, *69*, 188-188.
- [2] a) O. R. Pierce, Y. K. Kim, *Rubber Chem. Technol.* **1971**, *44*, 1350-1362; b) H. Maciejewski, A. Wawrzyńczak, M. Dutkiewicz, R. Fiedorow, *J. Mol. Catal. A: Chem.* **2006**, *257*, 141-148; c) B. Marciniak, E. Walczuk, P. Blazejewska-Chadyniak, D. Chadyniak, M. Kujawa-Welten, S. Krompiec, N. Auner, J. Weiss, *Wiley VCH, Weinheim* **2003**; d) Y. Morita, S. Tajima, H. Suzuki, H. Sugino, *J. Appl. Polym. Sci.* **2006**, *100*, 2010-2019; e) E. Beyou, P. Babin, B. Bennetau, J. Dunogues, D. Teyssie, S. Boileau, *J. Polym. Sci., Part A: Polym. Chem.* **1994**, *32*, 1673-1681; f) C. Iojoiu, M. J. Abadie, V. Harabagiu, M. Pinteala, B. C. Simionescu, *Eur. Polym. J.* **2000**, *36*, 2115-2123; g) Z. Li, J. Qin, Z. Yang, C. Ye, *J. Appl. Polym. Sci.* **2004**, *94*, 769-774; h) A. Sellinger, R. M. Laine, V. Chu, C. Viney, *J. Polym. Sci., Part A: Polym. Chem.* **1994**, *32*, 3069-3089; i) D. B. Drazkowski, A. Lee, T. S. Haddad, D. J. Cookson, *Macromolecules* **2006**, *39*, 1854-1863; j) A. Tuchbreiter, H. Werner, L. H. Gade, *Dalton Transactions* **2005**, 1394-1402.
- [3] a) D. Troegel, J. Stohrer, *Coord. Chem. Rev.* **2011**, *255*, 1440-1459; b) B. Marciniak, *Hydrosilylation: a comprehensive review on recent advances, Vol. 1*, Springer Science & Business Media, **2008**; c) T. Ganicz, T. Pakuła, W. A. Stańczyk, *J. Organomet. Chem.* **2006**, *691*, 5052-5055.
- [4] a) B. Boury, R. J. Corriu, D. Leclercq, P. H. Mutin, J. M. Planeix, A. Vioux, *Organometallics* **1991**, *10*, 1457-1461; b) A. Mori, H. Sato, K. Mizuno, T. Hiyama, K. Shintani, Y. Kawakami, *Chem. Lett.* **1996**, *25*, 517-518.

- 1
2
3
4 [5] a) M. J. O'brien, US Patent 6,531,540, **2003**; b) C. Herzig, B. Deubzer, D. Huettner, US
5 Patent 5,241,034, **1993**.
6
7
8
9
10 [6] a) H. Jyono, H. Odaka, H. Ito, H. Iwakiri, US Patent 6,444,775, **2002**; b) T. Watabe, T.
11 Matsumoto, T. Onoguchi, K. Tsuruoka, US Patent 6,207,766, **2001**.
12
13
14
15 [7] P. Jerschow, *Silicone elastomers, Vol. 137*, Smart Publications, **2001**.
16
17
18 [8] a) R. H. Morris, *Chem. Soc. Rev.* **2009**, 38, 2282-2291; b) B. K. Langlotz, H. Wadepohl,
19 L. H. Gade, *Angew. Chem. Int. Ed.* **2008**, 47, 4670-4674; c) S. C. Bart, E. Lobkovsky, P.
20 J. Chirik, *J. Am. Chem. Soc.* **2004**, 126, 13794-13807; d) I. Vankelecom, P. Jacobs,
21 *Catal. Today* **2000**, 56, 147-157.
22
23
24
25
26
27
28
29 [9] J. L. Speier, J. A. Webster, G. H. Barnes, *J. Am. Chem. Soc.* **1957**, 79, 974-979.
30
31
32 [10] B. Karstedt, US Patent 3,775,452, **1973**.
33
34
35 [11] a) M. Xue, J. Li, J. Peng, Y. Bai, G. Zhang, W. Xiao, G. Lai, *Appl. Organomet. Chem.*
36 **2014**, 28, 120-126; b) M. Igarashi, T. Matsumoto, T. Kobayashi, K. Sato, W. Ando, S.
37 Shimada, M. Hara, H. Uchida, *J. Organomet. Chem.* **2014**, 752, 141-146; c) H. Dong, Y.
38 Jiang, H. Berke, *J. Organomet. Chem.* **2014**, 750, 17-22; d) J. Y. Wu, B. N. Stanzl, T.
39 Ritter, *J. Am. Chem. Soc.* **2010**, 132, 13214-13216; e) P. B. Glaser, T. D. Tilley, *J. Am.*
40 *Chem. Soc.* **2003**, 125, 13640-13641; f) S. Nozakura, S. Konotsune, *Bull. Chem. Soc.*
41 *Jpn.* **1956**, 29, 326-331; g) L. Bareille, S. Becht, J. L. Cui, P. Le Gendre, C. Moïse,
42 *Organometallics* **2005**, 24, 5802-5806; h) S. Harder, J. Brettar, *Angew. Chem. Int. Ed.*
43 **2006**, 45, 3474-3478; i) V. Leich, T. P. Spaniol, L. Maron, J. Okuda, *Chem. Commun.*
44 **2014**, 50, 2311-2314.
45
46
47
48
49
50
51
52
53
54
55
56
57
58
59
60
61
62
63
64
65

- 1
2
3
4 [12] a) M. Rubin, T. Schwier, V. Gevorgyan, *J. Org. Chem* **2002**, *67*, 1936-1940; b) M. Pérez,
5
6 L. J. Hounjet, C. B. Caputo, R. Dobrovetsky, D. W. Stephan, *J. Am. Chem. Soc.* **2013**,
7
8 *135*, 18308-18310.
9
10
11 [13] a) I. E. Markó, S. Sterin, O. Buisine, G. Berthon, G. Michaud, B. Tinant, J. P. Declercq,
12
13 *Adv. Synth. Catal.* **2004**, *346*, 1429-1434; b) I. E. Markó, S. Stérin, O. Buisine, G.
14
15 Mignani, P. Branlard, B. Tinant, J.-P. Declercq, *Science* **2002**, *298*, 204-206; c) N.
16
17 Sabourault, G. Mignani, A. Wagner, C. Mioskowski, *Org. Lett.* **2002**, *4*, 2117-2119; d) L.
18
19 N. Lewis, K. G. Sy, G. L. Bryant Jr, P. E. Donahue, *Organometallics* **1991**, *10*, 3750-
20
21 3759; e) B. Marciniec, J. Guliński, *J. Organomet. Chem.* **1993**, *446*, 15-23.
22
23
24
25
26 [14] a) T. Galeandro-Diamant, M.-L. Zanota, R. Sayah, L. Veyre, C. Nikitine, C. de Bellefon,
27
28 S. Marrot, V. Meille, C. Thieuleux, *Chem. Commun.* **2015**, *51*, 16194-16196; b) B. P.
29
30 Chauhan, J. S. Rathore, *J. Am. Chem. Soc.* **2005**, *127*, 5790-5791; c) Y. Bai, S. Zhang, Y.
31
32 Deng, J. Peng, J. Li, Y. Hu, X. Li, G. Lai, *J. Colloid Interface Sci.* **2013**, *394*, 428-433.
33
34
35
36
37 [15] a) J. Stein, L. Lewis, Y. Gao, R. Scott, *J. Am. Chem. Soc.* **1999**, *121*, 3693-3703; b) T. K.
38
39 Meister, K. Riener, P. Gigler, J. r. Stohrer, W. A. Herrmann, F. E. Kühn, *ACS Catal.*
40
41 **2016**, *6*, 1274-1284.
42
43
44
45 [16] a) J. C. Bernhammer, H. V. Huynh, *Organometallics* **2013**, *33*, 172-180; b) J. J.
46
47 Dunsford, K. J. Cavell, B. Kariuki, *J. Organomet. Chem.* **2011**, *696*, 188-194; c) M. A.
48
49 Taige, S. Ahrens, T. Strassner, *J. Organomet. Chem.* **2011**, *696*, 2918-2927.
50
51
52
53 [17] B. Marciniec, K. Posala, I. Kownacki, M. Kubicki, R. Taylor, *ChemCatChem* **2012**, *4*,
54
55 1935-1937.
56
57
58
59 [18] C. M. Downing, H. H. Kung, *Catal. Commun.* **2011**, *12*, 1166-1169.
60
61
62
63
64
65

- 1
2
3
4 [19] a) Y. J. Chen, S. F. Ji, W. M. Sun, W. X. Chen, J. C. Dong, J. F. Wen, J. Zhang, Z. Li, L.
5
6 R. Zheng, C. Chen, Q. Peng, D. S. Wang, Y. D. Li, *J. Am. Chem. Soc.* **2018**, *140*, 7407-
7
8 7410; b) Y. Zhu, T. Cao, C. Cao, J. Luo, W. Chen, L. Zheng, J. Dong, J. Zhang, Y. Han,
9
10 Z. Li, C. Chen, Q. Peng, D. Wang, Y. Li, *ACS Catal.* **2018**, *8*, 10004-10011.
11
12
13
14 [20] A. J. Chalk, J. Harrod, *J. Am. Chem. Soc.* **1965**, *87*, 16-21.
15
16
17 [21] M. A. Schroeder, M. S. Wrighton, *J. Organomet. Chem.* **1977**, *128*, 345-358.
18
19
20 [22] a) S. Sakaki, N. Mizoe, M. Sugimoto, *Organometallics* **1998**, *17*, 2510-2523; b) S.
21
22 Sakaki, N. Mizoe, M. Sugimoto, Y. Musashi, *Coord. Chem. Rev.* **1999**, *190*, 933-960.
23
24
25 [23] a) Z. Huang, X. Gu, Q. Cao, P. Hu, J. Hao, J. Li, X. Tang, *Angew. Chem.* **2012**, *124*,
26
27 4274-4279; b) E. Fako, Z. Lodziana, N. Lopez, *Catal. Sci. Technol.* **2017**, *7*, 4285-4293;
28
29 c) Y. X. Chen, Z. W. Huang, Z. Ma, J. M. Chen, X. F. Tang, *Catal. Sci. Technol.* **2017**, *7*,
30
31 4250-4258.
32
33
34
35 [24] a) H. Sohn, J. Camacho-Bunquin, R. R. Langeslay, P. A. Ignacio-de Leon, J. Niklas, O.
36
37 G. Poluektov, C. Liu, J. G. Connell, D. Yang, J. Kropf, H. Kim, P. C. Stair, M.
38
39 Ferrandon, M. Delferro, *Chem. Commun.* **2017**, *53*, 7325-7328; b) W. Xu, Y. Li, B. Yu,
40
41 J. Yang, Y. Zhang, X. Chen, G. Zhang, Z. Gao, *J. Solid State Chem.* **2015**, *221*, 208-215;
42
43 c) M. D. Marcinkowski, J. Liu, C. J. Murphy, M. L. Liriano, N. A. Wasio, F. R. Lucci,
44
45 M. Flytzani-Stephanopoulos, E. C. H. Sykes, *ACS Catal.* **2016**, *7*, 413-420; d) B. Hu, A.
46
47 B. Getsoian, N. M. Schweitzer, U. Das, H. Kim, J. Nildas, O. Poluektov, L. A. Curtiss, P.
48
49 C. Stair, J. T. Miller, A. S. Hock, *J. Catal.* **2015**, *322*, 24-37; e) B. Qiao, A. Wang, X.
50
51 Yang, L. F. Allard, Z. Jiang, Y. Cui, J. Liu, J. Li, T. Zhang, *Nat. Chem.* **2011**, *3*, 634-641;
52
53 f) H. Yan, H. Cheng, H. Yi, Y. Lin, T. Yao, C. Wang, J. Li, S. Wei, J. Lu, *J. Am. Chem.*
54
55
56
57
58
59
60
61
62
63
64
65

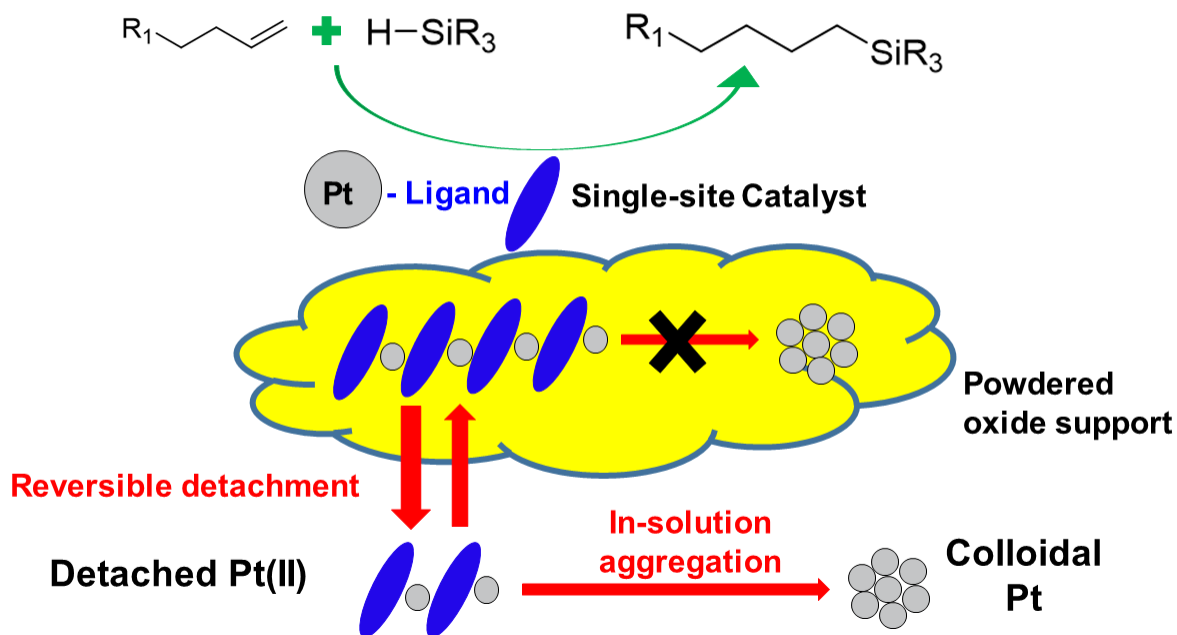
- 1
2
3
4 *Soc.* **2015**, *137*, 10484-10487; g) G. Vilé, D. Albani, M. Nachtegaal, Z. Chen, D.
5
6 Dontsova, M. Antonietti, N. López, J. Pérez- Ramírez, *Angew. Chem. Int. Ed.* **2015**, *54*,
7
8 11265-11269.
9
10
11
12 [25] L. Chen, G. E. Sterbinsky, S. L. Tait, *J. Catal.* **2018**, *365*, 303-312.
13
14
15 [26] a) D. Skomski, C. D. Tempas, K. A. Smith, S. L. Tait, *J. Am. Chem. Soc.* **2014**, *136*,
16
17 9862-9865; b) D. Skomski, C. D. Tempas, G. S. Bukowski, K. A. Smith, S. L. Tait, *J.*
18
19 *Chem. Phys.* **2015**, *142*, 101913; c) D. Skomski, C. D. Tempas, B. J. Cook, A. V.
20
21 Polezhaev, K. A. Smith, K. G. Caulton, S. L. Tait, *J. Am. Chem. Soc.* **2015**, *137*, 7898-
22
23 7902.
24
25
26
27
28 [27] J. L. Speier, in *Adv. Organomet. Chem.*, Vol. 17, Elsevier, **1979**, pp. 407-447.
29
30
31 [28] a) L. N. Lewis, R. J. Uriarte, N. Lewis, *J. Mol. Catal.* **1991**, *66*, 105-113; b) L. N. Lewis,
32
33 *J. Am. Chem. Soc.* **1990**, *112*, 5998-6004.
34
35
36
37 [29] a) L. N. Lewis, N. Lewis, *J. Am. Chem. Soc.* **1986**, *108*, 7228-7231; b) L. N. Lewis, R. J.
38
39 Uriarte, *Organometallics* **1990**, *9*, 621-625.
40
41
42 [30] a) W. Z. Wang, *Eur. Polym. J.* **2003**, *39*, 1117-1123; b) S. Y. Feng, M. Z. Cui, *Reactive*
43
44 *& Functional Polymers* **2000**, *45*, 79-83.
45
46
47
48 [31] a) A.-L. Brocas, C. Mantzaridis, D. Tunc, S. Carlotti, *Prog. Polym. Sci.* **2013**, *38*, 845-
49
50 873; b) H. Sugimoto, C. Kawamura, M. Kuroki, T. Aida, S. Inoue, *Macromolecules*
51
52 **1994**, *27*, 2013-2018; c) E. N. Jacobsen, *Acc. Chem. Res.* **2000**, *33*, 421-431.
53
54
55
56 [32] B. Marciniec, *Comprehensive handbook on hydrosilylation*, Elsevier, **2013**.
57
58
59
60
61
62
63
64
65

1
2
3
4
5
6
7
8
9
10
11
12
13
14
15
16
17
18
19
20
21
22
23
24
25
26
27
28
29
30
31
32
33
34
35
36
37
38
39
40
41
42
43
44
45
46
47
48
49
50
51
52
53
54
55
56
57
58
59
60
61
62
63
64
65

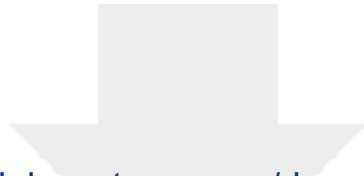
[33] C. D. Tempas, D. Skomski, B. J. Cook, D. Le, K. A. Smith, T. S. Rahman, K. G. Caulton, S. L. Tait, *Chem. Eur. J.* **2018**, *24*, 15852-15858.

[34] W. Kaim, J. Fees, *Z. Naturforsch., B: Chem. Sci.* **1995**, *50*, 123-127.

1
2
3
4 **Table of Contents entry**
5
6
7



Supported Pt single-site catalysts developed for alkene hydrosilylation using a metal-ligand coordination strategy offer improvements over nanoparticle and commercial catalysts. Pt single-sites are the main active species, which require activation but do not aggregate on supports. Fine tuning of metal centers is demonstrated by varying the ligand and the powdered oxide support.



Click here to access/download
Supporting Information
HSL Pt SSC SI v7.pdf

